An Integrated Optimization Framework for the Distribution Grid Expansion Planning

Francesco Moglia, Clément Moureau, Bertrand Cornélusse
Montefiore Institute
University of Liège
Liège, Belgium
francesco.moglia@uliege.be

***Abstract*—Distribution Networks are stressed by the mass adoption of distributed energy resources and new electric loads, leading to capacity issues, voltage limit violations, and volatility. An intelligent approach is needed as an alternative to costly brute-force reinforcement. This strategy focuses on increasing grid "smartness" and hosting capacity by using flexible operation and tariffs that incentivize flexible consumption, turning key assets into part of the solution. We adapt the Distribution Network Expansion Planning framework to embed network users' optimal investment and operation decisions for distributed assets. We address tariff design impact by comparing two strategies: a fully centralized formulation, with simultaneous network and user optimization, and a decentralized approach where user optimization precedes Distribution system operator decisions. The proposed method is applied to the design of a virtual campus electrical grid. To ensure computational tractability, we employ spatial reduction, representative day selection, and linearization techniques.**

***Index Terms*—Distribution network expansion planning, prosumer energy system sizing, grid tariff design.**

I. Introduction

Europe's electrification strategy faces a critical bottleneck in its Distribution Networks (DNs). Originally designed for unidirectional flow, DNs are now stressed by the mass adoption of distributed energy resources (DERs), like solar photovoltaics (PVs), and new electric loads such as electric vehicles (EVs) and heat pumps (HPs). This creates capacity issues, bidirectional flow challenges. While required physical upgrades are estimated at €400–€600 billion by 2030 [1], brute-force reinforcement is inefficient. An intelligent approach is necessary, focusing on increasing hosting capacity through flexible operation, market signals, and tariffs that incentivize flexible consumption. Key assets like EVs, batteries, and HPs must be part of the solution.

A. Literature review

Distribution Network Expansion Planning (DNEP) is the main framework for determining the most cost-effective strategy to reinforce the grid by selecting necessary upgrades to serve future demand while meeting all network constraints. As detailed in [2], this framework can be implemented in many ways: the demand forecast can range from deterministic worst-case scenarios [3] to complex probabilistic models accounting for multiple investment stages [4]. The portfolio of available grid upgrades can be limited to specific technologies or not: in the past, these upgrades were limited to conventional grid assets such as the installation or reinforcement of lines and substations [5], while in the last decade, DNEP models have incorporated Low-Carbon Technologies (LCTs) as investment alternatives, including the optimal sizing and siting of Distributed Generation (DG) and Energy Storage Systems (ESSs) [6], but also of EV charging infrastructure [7], [8]. More recently, the paradigm has begun to shift again to include non-network solutions, which use the intelligent operation of flexible resources as an alternative to costly physical upgrades [9]. Depending on the scope of the program and the modeling choices made, the problem's complexity can vary; thus, solution techniques range from exact optimization methods [10] to heuristic algorithms [11], [12].

The DNEP literature demonstrates a technical potential for finding highly efficient system solutions by co-optimizing network assets, LCTs, and non-network strategies. However, many of these advanced models are formulated from the perspective of a single, centralized planner with control over all assets. This approach often conflicts with the regulatory reality in the European Union, where DSOs are prohibited from owning and operating generation or storage [13]. In fact, the European regulatory body, ACER, defines price signal as the DSO's tool for steering network users towards patterns that incentivize grid-friendly behavior, enhance system-wide efficiency, and postpone the need for expensive grid reinforcements [14]. The challenge, therefore, is how to design price signals that effectively steer decentralized network users towards the system-wide efficiencies identified by centralized optimization models. To address this, game theory approaches can model the interactions between the different actors in the system, each with their own objectives and permissible actions [15], [16]. In this more realistic paradigm, DSOs steer the investment and operational decisions of other parties using indirect economic leverage. The most important of these instruments is the network tariff, i.e., the charges that are necessary to cover the network's capital and operational costs and, crucially, to promote the efficient use of the grid. Alongside tariffs, new mechanisms like local flexibility markets are emerging as a similar tool to procure grid services from LCTs owners. This highlights a key connection: if DSOs must rely on economic signals to unlock the value of flexibility, it is essential to understand which tariff schemes are most effective.

B. Contributions

The core contribution of this paper is the adaptation of the DNEP framework to systematically embed network users' optimal investment and operation decisions regarding distributed assets. In particular, the proposed DNEP formulation comprises two voltage levels and the possibility of installing statcoms to regulate reactive power. We address the crucial questions of tariff design and its influence on network development by implementing and comparing two distinct optimization strategies: a fully centralized formulation, which optimizes network reinforcement and user decisions simultaneously, and a decentralized approach, where users first optimize their assets, and the Distribution System Operator (DSO) then makes network decisions. Furthermore, we introduce and evaluate several approximation schemes to ensure the computational tractability of these complex planning problems: a spatial reduction technique to limit the scope of possible network investments, a representative days selection mechanism to manage temporal complexity, and several linearization techniques applied to the underlying mathematical formulation.

C. Organization

Section II summarizes the general methodology, Section III details the mathematical model, Section IV presents the use case, while Section V explains and evaluates the approximations used to reduce computation time. Section VI reports results for a virtual campus under various tariff scenarios. Section VII concludes.

II. Methodology

We present a comparative optimization framework to quantify the *value of coordination* in distribution grids and assess the influence of tariff structures. Coordination denotes consumers' ability to adjust their net electricity exchange through investment and operation of LCTs such as PV, ESSs, and inverters with dynamic power control.

The framework contrasts two planning scenarios, each coupling a detailed DNEP with a prosumer energy system sizing and operation model for each load bus. In the *Centrally Optimized Scenario*, an omniscient planner jointly optimizes all grid and LCT decisions to minimize total system cost, while in the *Decentralized Scenario*, consumers act independently to minimize their own bills under a given tariff, while the DSO reinforces the grid to maintain feasibility.

The resulting *total system cost gap* between the two scenarios measures the *economic value of coordination*, i.e., the cost reduction attainable through perfectly aligned decisions. This value serves to:

- compare and design tariff structures that promote coordinated behavior,
- evaluate LCT operation strategies, and
- define a rational basis for pricing flexibility services.

Although the framework does not directly optimize tariffs, it identifies those that yield efficient, system-wide outcomes by linking flexibility to avoided grid reinforcement costs.

III. Mathematical models

This section details the DNEP and prosumer energy system sizing and operation mathematical models and how we combine them. The notation is detailed in the appendix.

A. Distribution Network Expansion Planning

The objective is to minimize the total annualized cost, which includes the investment in medium (MV) and low voltage (LV) grid assets, i.e. substations, cables, and statcoms, and the cost of energy imported at the High Voltage (HV) substation. This objective is offset by revenues from user bills, which are a function of their consumption and the specific tariff scheme. Additionally, penalties are applied to avoid any operational violations and to enforce a radial network topology. The DNEP model is founded on the DistFlow equations [17] (1c). Operational limits (1d) ensure that bus voltages remain within a secure range and that line currents do not exceed thermal ratings while also fixing to 1 p.u. the voltage of active HV substations. The group of constraints (1e) links binary investment decisions to physical constraints, including power flow limits per conductor, aggregation to total line flow, and the quadratic capacity ratings for substations. Constraints (1f) enforce the power balance at all node types. Finally, a set of constraints (1g) uses a fictitious commodity flow to ensure the final grid design is connected and radial.

$$\min \quad C_{grid} + C_{import} - C_{revenue} + C_{pen} \tag{1a}$$

$$\begin{aligned}
\text{s.t.} \quad & C_{grid} = \frac{1}{T_{horizon}} \Bigg(\sum_{l,c} \delta_{l,c} \pi_{l,c} \\
& + \sum_{s_{hv}} (S_{s_{hv}} \pi_{s_{hv}} + \beta_{s_{hv}} f_{s_{hv}}) \\
& + \sum_{s_{mv}} (S_{s_{mv}} \pi_{s_{mv}} + \gamma_{s_{mv}} f_{s_{mv}}) \\
& + \sum_{b} (Q_{scom_b} \pi_{scom} + \mu_{scom_b} f_{scom_b}) \Bigg) \\
& C_{import} = \sum_{p,s_{hv}} P_{p,s_{hv}} \cdot \pi_{import} \\
& C_{revenue} = \sum_{b} f(P_{bus,p,b}, Q_{bus,p,b}) \\
& C_{pen} = C_{penalty} \cdot \left(\sum_{p,l,c} \Delta i^2_{p,l,c} + \sum_{b} F_{unserved,b} \right)
\end{aligned} \tag{1b}$$

$$\begin{aligned}
& v^2_{p,j} - v^2_{p,i} = -2 \sum_{c} (r_{l,c} P_{p,l,c} + x_{l,c} Q_{p,l,c}) \\
& + (r^2_{l,c} + x^2_{l,c}) i^2_{p,l,c}, \ \forall p, l = (i,j) | \alpha_l = 1 \\
& v^2_{p,i} \cdot i^2_{p,l} \geq P^2_{p,l} + Q^2_{p,l}, \ \forall p, l = (i,j) \\
& Loss_{p,l} = \sum_{c} r_{l,c} \cdot i^2_{p,l,c}, \ \forall p, l
\end{aligned} \tag{1c}$$

$$\begin{aligned}
& V^2_{min} \leq v^2_{p,j} \leq V^2_{max}, \ \forall p, j \in \mathcal{B} \cup \mathcal{S}_{MV} \\
& i^2_{p,l,c} - \Delta i^2_{p,l,c} \leq I^2_{max,c} \cdot \delta_{l,c}, \ \forall p, l, c \\
& v^2_{p,s_{hv}} = 1, \ \forall p, s_{hv} | \beta_{s_{hv}} = 1
\end{aligned} \tag{1d}$$

$$\alpha_l = \sum_{c \in \mathcal{C}} \delta_{l,c},\ \forall l$$
$$|P_{p,l,c}| \leq \delta_{l,c} \cdot I_{max,c} \cdot V_{max},\ \forall p, l, c$$
$$|Q_{p,l,c}| \leq \delta_{l,c} \cdot I_{max,c} \cdot V_{max},\ \forall p, l, c$$
$$\forall p, l,$$
$$P_{p,l} = \sum_{c \in \mathcal{C}} P_{p,l,c};\ Q_{p,l} = \sum_{c \in \mathcal{C}} Q_{p,l,c};\ i^2_{p,l} = \sum_{c \in \mathcal{C}} i^2_{p,l,c}$$
$$\beta_{s_{hv}} \cdot S^2_{s_{hv}} \geq P^2_{p,s_{hv}} + Q^2_{p,s_{hv}},\ \forall p, s_{hv}$$
$$\gamma_{s_{mv}} \cdot S^2_{s_{mv}} \geq P^2_{p,s_{mv}} + Q^2_{p,s_{mv}},\ \forall p, s_{mv}$$
$$|Q_{scom,p,b}| \leq \mu_{scom_b} Q_{scom_b},\ \forall p, b \tag{1e}$$
$$\forall p, s_{hv}$$
$$P_{p,s_{hv}} = \sum_{l \in \mathcal{L}^{from}_{s_{hv}}} P_{p,l} - \sum_{l \in \mathcal{L}^{to}_{s_{hv}}} (P_{p,l} - \sum_c r_{l,c} \cdot i^2_{p,l,c})$$
$$Q_{p,s_{hv}} = \sum_{l \in \mathcal{L}^{from}_{s_{hv}}} Q_{p,l} - \sum_{l \in \mathcal{L}^{to}_{s_{hv}}} (Q_{p,l} - \sum_c i^2_{p,l,c} x_{l,c})$$
$$\forall p, s_{mv}$$
$$\sum_{l \in \mathcal{L}^{from}_{s_{mv}}} P_{p,l} = \sum_{l \in \mathcal{L}^{to}_{s_{mv}}} (P_{p,l} - \sum_c r_{l,c} \cdot i^2_{p,l,c})$$
$$\sum_{l \in \mathcal{L}^{from}_{s_{mv}}} Q_{p,l} = \sum_{l \in \mathcal{L}^{to}_{s_{mv}}} (Q_{p,l} - \sum_c i^2_{p,l,c} x_{l,c})$$
$$P_{p,s_{mv}} = \sum_{l \in \mathcal{L}^{fromLV}_{s_{mv}}} P_{p,l} - \sum_{l \in \mathcal{L}^{toLV}_{s_{mv}}} (P_{p,l} - \sum_c r_{l,c} \cdot i^2_{p,l,c})$$
$$Q_{p,s_{mv}} = \sum_{l \in \mathcal{L}^{fromLV}_{s_{mv}}} Q_{p,l} - \sum_{l \in \mathcal{L}^{toLV}_{s_{mv}}} (Q_{p,l} - \sum_c i^2_{p,l,c} x_{l,c})$$
$$\forall p, b$$
$$P_{bus,p,b} = \sum_{l \in \mathcal{L}^{from}_b} P_{p,l} - \sum_{l \in \mathcal{L}^{to}_b} (P_{p,l} - \sum_c r_{l,c} \cdot i^2_{p,l,c})$$
$$Q_{bus,p,b} = Q_{scom,p,b} + \sum_{l \in \mathcal{L}^{from}_b} Q_{p,l} - \sum_{l \in \mathcal{L}^{to}_b} (Q_{p,l} - \sum_c i^2_{p,l,c} x_{l,c}) \tag{1f}$$
$$1 - F_{unserved,b} = \sum_{l \in \mathcal{L}^{to}_b} F_l - \sum_{l \in \mathcal{L}^{from}_b} F_l,\ \forall b$$
$$F_{s_{hv}} = \sum_{l \in \mathcal{L}^{from}_{s_{hv}}} F_l - \sum_{l \in \mathcal{L}^{to}_{s_{hv}}} F_l,\ \forall s_{hv}$$
$$\sum_{l \in \mathcal{L}^{to}_{s_{mv}}} F_l = \sum_{l \in \mathcal{L}^{from}_{s_{mv}}} F_l,\ \forall s_{mv}$$
$$\hat{\gamma}_{s_{mv}} \leq \sum_{l \in \mathcal{L}_{s_{mv}}} \alpha_l,\ \forall s_{mv}$$
$$|F_l| \leq \alpha_l \cdot |\mathcal{B}| \quad \forall l; \quad F_{s_{hv}} \leq \beta_{s_{hv}} \cdot |\mathcal{B}|,\ \forall s_{hv}$$
$$\sum_{l \in \mathcal{L}} \alpha_l = \sum_{b \in \mathcal{B}} 1 + \sum_{s_{hv} \in \mathcal{S}_{hv}} \beta_{s_{hv}} + \sum_{s_{mv} \in \mathcal{S}_{mv}} \hat{\gamma}_{s_{mv}} - 1 \tag{1g}$$

B. Prosumer energy system sizing and operation

The prosumer problem (2) determines the optimal investment in and operation of LCTs for each bus. It decides the optimal size of PV panels, ESSs, and inverters, as well as their hourly dispatch, to satisfy the local load ($P_{load,p,b}, Q_{load,p,b}$). The objective minimizes the total cost, including the cost of the installed asset and the cost of the energy, the latter being defined as a function of the net exchanged power and the tariffs. The key variables, $P_{bus,p,b}$ and $Q_{bus,p,b}$, represent the net power that the bus must draw from or inject into the grid. They are used as input parameters for the DNEP program when the problems are solved sequentially. The energy system is modeled with an AC and a DC bus connected by a single inverter. The AC bus is where the load and the grid are connected, while the PV system and storage are on the DC bus. Each bus has its own power balance constraint: (2d) for the AC side and (2g) for the DC side. As for the single assets, the PV system model (2e) limits the installed panel area to the available surface and links their generation to solar irradiance. The energy storage system constraints (2f) manage the battery's state of charge, linking it to charging/discharging powers and enforcing a daily cyclical energy balance. Finally, all these constraints also link the operational variables to the asset sizes.

$$\min \quad C_{asset,b} + C_{elec,b} \tag{2a}$$
$$\text{s.t.} \quad C_{asset,b} = \frac{1}{T_{horizon}} \Big(A_{pv,b}\pi_{pv} + E_{stor,b}\pi_{storage} + S_{inv,b}\pi_{inverter} + \pi_b f_{pv} + \sigma_b f_{storage} \Big) \tag{2b}$$
$$C_{elec,b} = f(P_{bus,p,b}, Q_{bus,p,b}) \tag{2c}$$
$$P_{bus,p,b} = P_{load,p,b} - P_{inv,p,b},\ \forall p$$
$$Q_{bus,p,b} = Q_{load,p,b} - Q_{inv,p,b},\ \forall p \tag{2d}$$
$$A_{pv,b} \leq A^{max}_b \cdot \pi_b,\ \forall b$$
$$P_{pv,p,b} \leq A_{pv,b} \cdot I_p \cdot \eta_{pv},\ \forall p \tag{2e}$$
$$E_{stor,b} \leq E^{max}_{stor} \cdot \sigma_b,\ \forall b$$
$$E_{p,b} \leq E_{stor,b},\ \forall p$$
$$\forall p : (p-1)\%24 \neq 0$$
$$E_{p,b} = E_{p-1,b} + (\eta_{stor} P_{ch,p,b} - \frac{1}{\eta_{stor}} P_{dis,p,b})\Delta t$$
$$\forall p : (p-1)\%24 = 0$$
$$E_{p,b} = E_{p+23,b} \tag{2f}$$
$$S^2_{inv,b} \geq P^2_{inv,p,b} + Q^2_{inv,p,b},\ \forall p$$
$$P_{pv,p,b} + P_{dis,p,b} = P_{inv,p,b} + P_{ch,p,b},\ \forall p \tag{2g}$$

C. The Unified Centralized Model

The centrally optimized scenario defined in Section II gathers the models (1) and (2). $P_{bus,p,b}$ and $Q_{bus,p,b}$ then become endogenous variables co-optimized with all other variables. The objective becomes the sum of the objective functions from models (1) and (2). It is independent of tariffs: considering the two problems from a central planner's perspective, the money exchange between the DSO and the users sums up to zero.

TABLE I
PROPERTIES OF DIFFERENT CONDUCTORS

Conductors	q mm^2	r Ω/km	x_l Ω/km	i_{max} kA	**cost** k€/km
Aster	16	1.15	0.32	0.10	90
Iris	35	0.52	0.30	0.18	125
Violet	70	0.26	0.28	0.28	190
Lupin	120	0.15	0.26	0.38	275
Peony	185	0.10	0.24	0.52	400

IV. USE CASE

To test our model, we use a dataset of synthetic campuses. These span a maximum area of 9 km^2, and contain between 35 and 55 load buses, which draw between 3 and 5 MW of peak power. Each campus in the dataset features the geographical coordinates of a single primary substation (HV) and of a set of load buses at either medium or low voltage level, each of which comes with active and reactive power profiles at an hourly resolution. Additionally, the irradiance vector together with surface area (A_b^{max}) for each bus defines the renewable potential. Finally, the buses are also grouped into distinct districts, which aids in structuring the network design.

The analysis is performed using a greenfield approach, meaning the distribution network is designed from scratch rather than modifying an existing one. This was a deliberate choice to remove the confounding influence of legacy infrastructure. To allow our model to design the network connecting the primary substation to every load, we must integrate the dataset with the candidate option for network asset: comprehensive sets for secondary substations, line routes, and conductors must be defined so that the model can choose which of them to build. The placement of secondary (MV/LV) substations is a critical design decision. To provide the model with a set of viable options without pre-determining the outcome, we randomly select three candidate locations within each district to host a potential secondary substation. We define a set of candidate conductors with a broad range of capacities (Table I). Finally, since we follow a greenfield approach, the complete graph is initially considered.

V. APPROXIMATION SCHEMES AND EVALUATION

The complete formulation comprises approximately 60 million variables, of which about 2,000 are binary. This scale makes the problem not only memory-intensive but also combinatorially hard. Running the optimization over the full temporal and spatial resolution would be computationally prohibitive given the available resources (i7-13620H, 16GB RAM). Therefore, approximation and reduction techniques were applied to obtain a tractable problem size.

A. Spatial Reduction

The combinatorial explosion of the problem is primarily driven by the number of candidate lines; hence, two pruning techniques are evaluated to reduce the complete graph.

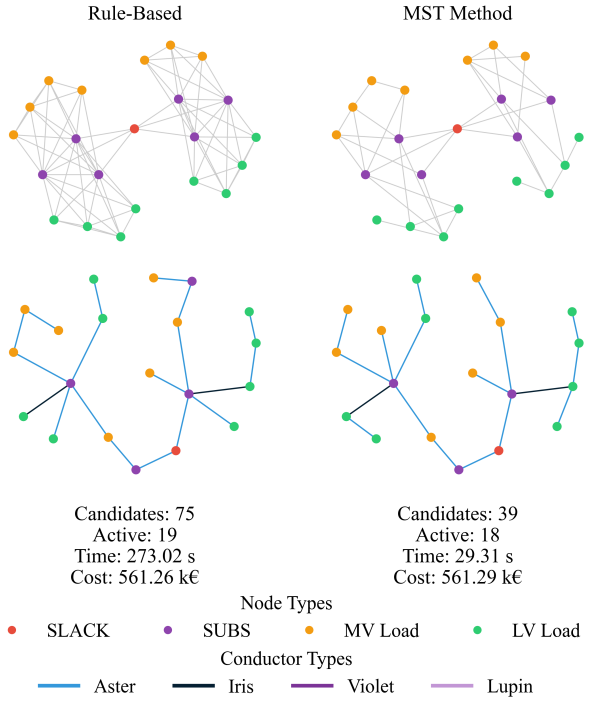

Fig. 1. Candidate lines and results for the two spatial reduction methods.

1) Rule-Based Heuristic:

- Connect every HV substation to every MV substation.
- Connect MV substations within the same district to provide redundancy.
- Connect each MV substation to all MV and LV loads located within the same district.
- Connect each MV load to its two geographically closest MV load neighbors within the same district.
- Connect each LV load to its two geographically closest LV load neighbors within the same district.

2) Minimum Spanning Tree (MST) based Reduction: This method starts from the set of lines generated by the rule-based heuristic, then iteratively considers each substation as the sole source and finds the shortest possible set of lines (a spanning tree) to connect all loads. By repeating this for every potential substation and combining the resulting trees, we ensure the final candidate set contains the shortest paths, regardless of which substations are ultimately chosen.

Figure 1 compares the two methods. Model (1) is configured to run on two districts, for a single time step, using the base load for each bus. This simplification isolates the effect of the candidate line set on the resulting topology and computational performance. The resulting optimal network topologies show that the rule-based heuristic only removes 3 candidate lines out of the total of 78, while the optimal solution found is identical to the full search space, the solving time is not improved. On the other hand, using the MST method reduces the candidate lines to 39, which has a great benefit in terms of solving time, although the reduced search space pruned the optimal solution and the objective is slightly above the global minimum.

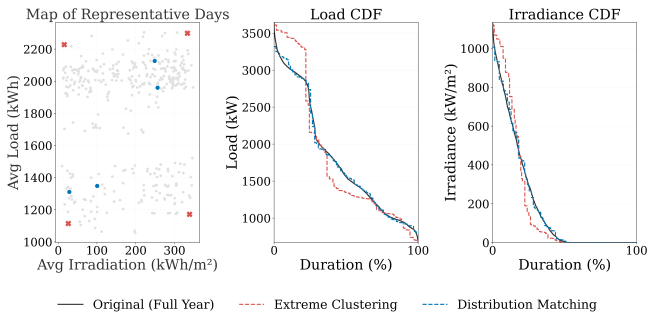

Fig. 2. Illustration of the two temporal reduction techniques.

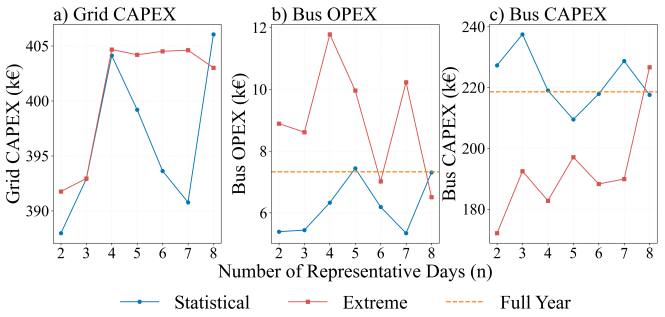

Fig. 3. Comparison of CAPEX and OPEX for the DSO and Grid User under extreme and statistical day selection methods.

B. Temporal Reduction: Representative Day Selection

Running the optimization model over a full year is computationally infeasible. However, isolating a single critical timestep would eliminate temporal coupling and make it impossible to model storage dynamics. Therefore, a reduced set of representative days must be selected. This reduction inevitably alters the optimization outcome, as the selected subset cannot perfectly reproduce the temporal diversity of the full year. The objective is therefore to minimize this distortion. To this end, we compare two methods for temporal reduction, each emphasizing a different aspect of fidelity, both based on the aggregated electricity demand and solar irradiance annual time series.

1) Statistical Distribution Matching: This optimization-based method selects a small, weighted set of days whose combined statistical properties closely reproduce those of the full annual data [18]. By minimizing the deviation between the cumulative distribution functions (CDFs) of the full year and the selected subset, it preserves the frequency and magnitude of operating conditions, ensuring that the resulting operational costs (OPEX) remain close to those of the full-year simulation.

2) Extreme Day Selection: This clustering-based method prioritizes network robustness over reproducing operational cost distributions. All 365 days are grouped into clusters based on aggregated demand and solar irradiance profiles. From each cluster, the "extreme" day—defined as the day furthest from the cluster center—is selected. By designing the grid to withstand these extreme conditions, the method increases the likelihood that the resulting network will perform reliably under all conditions throughout the year, thus helping to preserve the true grid cost (CAPEX).

The model was run on one district, using an increasing number of representative days. For this experiment, a simple tariff scheme was used where grid users only pay for their net consumed energy at the wholesale market price. The resulting designs are then evaluated based on their total CAPEX and the OPEX for both the DSO and grid users. Figure 3 highlights the trade-off between designing for cost-efficiency versus resilience.

The extreme days method tends to capture more stressful operating conditions, often leading to higher grid CAPEX. It also shows greater variability in OPEX, while the statistical method remains closer to full-year results.

C. Linearization of the MINLP Model

This section details the different non-linearities that are not trivial to linearize and the implemented linearization techniques together with a set of experiments to address their performance and tune their parameters.

a) Polygonal Approximation of Circular Constraints: The linearization of the quadratic relationship $z^2 \geq x^2 + y^2$, which applies to asset rating constraints, is achieved by replacing the single quadratic constraint with N linear inequalities, modeling the circular feasible region as an N−sided regular polygon. To ensure a conservative approximation, the polygon is inscribed within the circle. To accomplish this, constraints are scaled by a factor of $\cos(\pi/N)$:

$$z \cdot \cos\left(\frac{\pi}{N}\right) \geq a_k x + b_k y \quad \forall k = 1, \ldots, N \tag{3}$$

where $a_k = \cos(2\pi k/N)$ and $b_k = \sin(2\pi k/N)$. The trade-off is between precision (higher N) and computational cost. We compare this inner linearization (scaled polygon) with an exterior approximation (scale factor = 1) Figure 4 reveals a

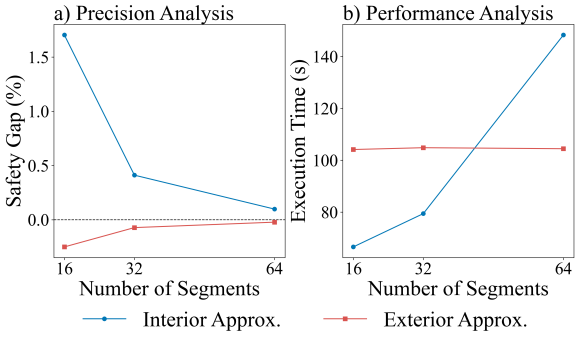

Fig. 4. Time performance and precision of polygonal linearization, comparing the interior and exterior polygonal approximations using increasing number of segments.

critical trade-off between computational cost, precision, and operational safety. Panel (a) highlights how our proposed interior approximation consistently produces a positive "Safety

Gap," guaranteeing that the system's capacity is never overestimated. In stark contrast, the exterior approximation falls into the non-conservative, unsafe region. The performance trade-offs are detailed in panel (b).

b) Piecewise Linearization of the Square Function: A key non-linearity arises from the apparent power constraint:

$$v_{p,i}^2 \cdot i_{p,l}^2 \geq P_{p,l}^2 + Q_{p,l}^2.$$

We build upon the piecewise linearization method proposed in [19], combining voltage approximation and linearization of the square function.

1) **Voltage approximation.** Since the voltage range is narrow ($V \in [0.95; 1.05]\, p.u.$), it is approximated to 1, removing the bilinear term and yielding $i_{p,l}^2 \geq P_{p,l}^2 + Q_{p,l}^2$.
2) **Absolute power linearization.** Because $x^2 = (-x)^2$, active and reactive powers are expressed through non-negative variables $P_{p,l}^+, P_{p,l}^-$ and $Q_{p,l}^+, Q_{p,l}^-$, such that $|P_{p,l}| = P_{p,l}^+ + P_{p,l}^-$ and $|Q_{p,l}| = Q_{p,l}^+ + Q_{p,l}^-$.
3) **Domain discretization.** The absolute power domain $[0, X_{max,l}]$ is divided into n contiguous segments indexed by $d \in \mathcal{D}$. Each has width $LPWB_{l,d}$ and slope $SPWB_{l,d}$ given by

$$SPWB_{l,d} = \frac{X_{end}^2 - X_{start}^2}{X_{end} - X_{start}} = X_{start} + X_{end}. \quad (4)$$

4) **Linear reformulation.** The non-linear constraint is replaced by:

$$|P_{p,l}| = \sum_{d \in \mathcal{D}} P_{p,l,d}, \quad |Q_{p,l}| = \sum_{d \in \mathcal{D}} Q_{p,l,d}, \quad (5)$$

$$0 \leq P_{p,l,d}, Q_{p,l,d} \leq LPWB_{l,d}, \quad (6)$$

$$i_{p,l}^2 \geq \sum_{d \in \mathcal{D}} SPWB_{l,d}(P_{p,l,d} + Q_{p,l,d}). \quad (7)$$

While this formulation follows [19], we observed that the definition of segment lengths $LPWB_{l,d}$ strongly affects precision. To improve accuracy, we tested two alternatives—*constant* and *logarithmic progression* segment lengths—and compared their performance.

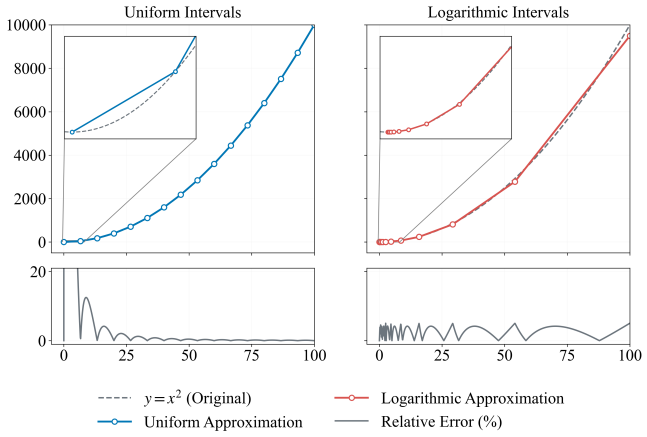

Fig. 5. Precision of the square function linearization using constant and logarithmic segment lengths.

As shown in Figure 5, the logarithmic method yields a more uniform relative error, providing a more accurate approximation. Its advantage is confirmed in our application test, Figure 6, where it achieves a relative current error below 20% while maintaining comparable computation times.

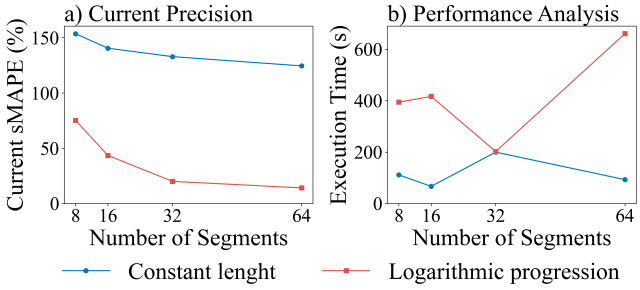

Fig. 6. Comparison of linearization methods in terms of accuracy and computation time.

c) Linearization of Indicator Constraints: The Big-M Method: Finally, we tackle the logical "if-then" constraints, such as the DistFlow equations holding only for active lines ($\alpha_l = 1$), using the Big-M method. For an equality constraint like $g(x) = h(x)$, this method consists in first decomposing the constraint into two inequalities: $g(x) \leq h(x)$ and $g(x) \geq h(x)$. Then we respectively add and subtract the Big-M term to the obtained inequalities. For the DistFlow voltage drop equation, this results in:

$$\begin{aligned} v_{p,j}^2 - v_{p,i}^2 \leq -2 \sum_c (r_{l,c} P_{p,l,c} + x_{l,c} Q_{p,l,c}) \\ + (r_{l,c}^2 + x_{l,c}^2) i_{p,l,c}^2 + M \cdot (1 - \alpha_l) \\ v_{p,j}^2 - v_{p,i}^2 \geq -2 \sum_c (r_{l,c} P_{p,l,c} + x_{l,c} Q_{p,l,c}) \\ + (r_{l,c}^2 + x_{l,c}^2) i_{p,l,c}^2 - M \cdot (1 - \alpha_l) \end{aligned}$$

When $\alpha_l = 1$, the M terms become zero, enforcing the original equality. When $\alpha_l = 0$, the large M value makes the constraints non-binding.

1) Heuristic for Accelerated Convergence: Even with all the precited complexity reduction techniques, our problem remains large and difficult. Hence we developed a heuristic to provide a high-quality initial solution:

1) **Initial Run:** The model is first solved considering only the best (and most expensive) conductor type for all lines.
2) **Fix Topology:** The resulting optimal topology is fixed.
3) **Iterative Downgrade:** the conductor type on the least-loaded lines are downgraded, re-running the optimization after each change to check feasibility and total cost.
4) **Select Best Guess:** The feasible configuration with the lowest total cost is selected and can be fed to the full optimization program as a warm start.

VI. Planning results

A. Scenarios

We apply our methodology to test different tariff designs, which can be based on consumed/injected energy, maximum drawn power, or a mix of both. For energy rates, net metering tariffs have equivalent injection π^{exp} and consumption π^{imp} fees, allowing users to offset consumed energy with injected energy over different timesteps. Net billing tariffs remunerate injected energy at a rate lower than the import price ($\pi^{imp} > \pi^{exp}$). Finally, capacity tariffs, based on maximum drawn power, can be a small yearly fee (π^{cap}) or the main component of the bill. Table II summarizes the scenarios analyzed.

TABLE II
Definition of scenarios.

Scenario	π^{imp} €/kWh	π^{exp} €/kWh	π^{cap} €/kW
Net metering	0.03	0.03	0
Net billing low spread	0.03	0.015	0
Net billing high spread	0.045	0.005	0
Net billing with capacity fee	0.03	0.015	0.2
Net billing with high capacity fee	0.03	0.015	0.4
Net metering with capacity fee	0.03	0.03	0.2
Net metering with high capacity fee	0.03	0.03	0.4

B. Numerical results

We compare the centralized model with the distributed model for each tariff. The cost of imported electricity varies between 95 and 106 k€/year and represents around 70%. of the yearly cost. The variation is partly caused by curtailment of PV production driven by additional cost related to capacity fees. The remaining difference in electricity cost stems from the different operation of ESSs and thus the different values of energy losses connected with those assets.

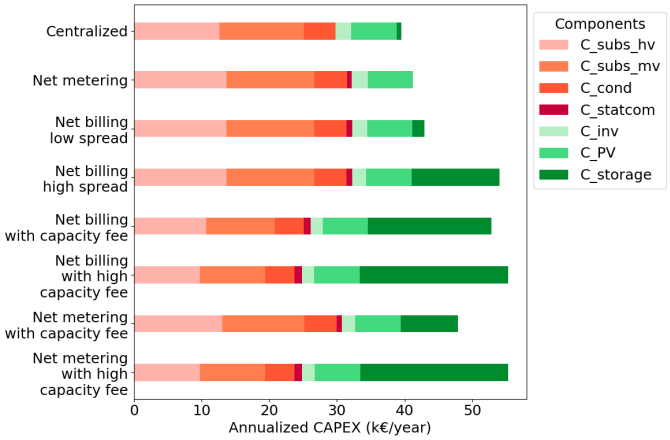

Fig. 7. Annualized cost comparison by scenario.

The analysis of annualized CAPEX, Figure 7 highlights how tariff design fundamentally shapes both the installation and operational strategies of distributed storage, with direct implications for grid investment needs.

In the centralized case, a modest amount of storage is deployed. Its operation is coordinated to smooth demand peaks, achieving an effective trade-off between storage investment and savings in grid reinforcement. This centralized control effectively invests in LCTs to minimize grid stress, leading to the lowest overall CAPEX.

Moving to net metering, storage installations drop to zero. Since prosumers can withdraw electricity from the grid at the same price as they inject it, they effectively use the grid as a virtual battery. Individual storage becomes economically unjustified, and the grid must accommodate all temporal imbalances, resulting in an increase of CAPEX of 3.5%.

Under net billing, the incentive structure changes. The spread between export and import tariffs encourages users to install batteries, allowing them to avoid paying the tariff differential by storing excess PV generation for later self-consumption. However, this self-centered strategy does not alleviate grid congestion. Storage operation follows economic arbitrage rather than grid support objectives—thus, on days without PV production, storage provides no relief to the network. Consequently, although total CAPEX rises due to higher storage deployment, grid-related costs remain nearly unchanged.

Introducing a capacity fee produces a markedly different behavior. Storage adoption increases substantially, as users exploit it to flatten their consumption profiles and minimize peak-demand charges. Unlike in previous cases, this mode of operation directly mitigates grid stress, substantially lowering the required grid investments. However, the overall system cost rises because deploying distributed storage is more expensive than reinforcing grid assets, as done in the centralized scenario.

Turning to reactive power management, we observe that all scenarios except the centralized one require statcom installations. In the centralized configuration, reactive power compensation is handled by the inverter fleet, whose control capabilities maintain voltages within operational limits without additional equipment. Interestingly, inverter costs remain relatively stable across scenarios-69 k€ in the centralized case versus 55–60 k€ elsewhere, except for net metering at 71 k€ due to the absence of battery coupling to the DC bus.

In decentralized cases, users have no economic incentive or visibility to provide reactive power support, even though their inverters are technically capable of doing so. As a result, the grid operator must install dedicated statcoms—adding roughly 35 k€ in capital expenditure—to ensure voltage stability. This leads to an inefficiency: users invest in inverters that could already deliver this service, but, lacking appropriate price signals or coordination, the same capability is replicated at the grid level.

VII. Conclusion and future work

This article presented a model to analyze the impact of different grid tariff designs on both grid investments and end-user behavior. Applied to a greenfield case, the model was validated by reproducing qualitative trends reported in

previous studies using independent methodologies. In particular, it confirms that net metering discourages local storage adoption and increases reliance on the grid, while capacity-based tariffs effectively promote demand flattening and grid stress reduction. At the same time, the analysis reveals that under limited solar potential, net billing does not significantly alleviate grid stress, and that billing users solely on active power does not incentivize a smart or efficient use of inverter capabilities.

These results are specific to the cost assumptions and the case study considered. Changes in technology or grid equipment costs could alter the quantitative outcomes. Moreover, the present analysis excludes emerging loads from electric heating (heat pumps) and transport (EVs), and does not explicitly account for certain forms of demand-side flexibility, such as direct load control. Nonetheless, the model has been designed for extensibility, enabling straightforward integration of new load profiles and adaptation to brownfield planning contexts. Future work will focus on incorporating these additional loads and flexibility mechanisms to assess their influence on tariff design and grid investment strategies.

REFERENCES

[1] S. Butorac, "*EU electricity grids*," European Parliamentary Research Service, European Parliament, Brussels, Briefing PE 772.854, 2025.

[2] T. D. de Lima, F. Lezama, J. Soares, J. F. Franco, and Z. Vale, "Modern distribution system expansion planning considering new market designs: Review and future directions," *Renewable and Sustainable Energy Reviews*, vol. 202, p. 114709, 2024.

[3] J. M. Nahman and D. M. Peric, "Optimal planning of radial distribution networks by simulated annealing technique," *IEEE Transactions on Power Systems*, vol. 23, no. 2, pp. 790–795, may 2008.

[4] A. Soroudi, A. Keane, and M. Power, "Multi-stage rolling grid expansion planning for distribution networks considering conditional value at risk," *IEEE Transactions on Power Systems*, vol. 27, no. 3, pp. 1583–1592, aug 2012.

[5] J. F. Franco, M. J. Rider, and R. Romero, "A mixed-integer quadratically-constrained programming model for the distribution system expansion planning," *Electrical Power and Energy Systems*, vol. 62, pp. 265–272, 2014.

[6] G. Muñoz-Delgado, J. Contreras, and J. M. Arroyo, "Joint expansion planning of distributed generation and distribution networks," *IEEE Transactions on Power Systems*, vol. 30, no. 5, pp. 2579–2590, sep 2015.

[7] M. A. Mejía, L. H. Macedo, G. Munoz-Delgado, J. Contreras, and A. Padilha-Feltrin, "Multistage planning model for active distribution systems and electric vehicle charging stations considering voltage-dependent load behavior," *IEEE Transactions on Smart Grid*, vol. 13, no. 2, pp. 1383–1397, mar 2022.

[8] H. Yao, Y. Xiang, C. Gu, and J. Liu, "Optimal planning of distribution systems and charging stations considering pv-grid-ev transactions," *IEEE Transactions on Smart Grid*, vol. 16, no. 1, pp. 691–704, jan 2025.

[9] A. Arefi, A. Abeygunawardana, and G. Ledwich, "A new risk-managed planning of electric distribution network incorporating customer engagement and temporary solutions," *IEEE Transactions on Sustainable Energy*, vol. 7, no. 4, pp. 1646–1661, oct 2016.

[10] H. Haghighat and B. Zeng, "Stochastic and chance-constrained conic distribution system expansion planning using bilinear benders decomposition," *IEEE Transactions on Power Systems*, vol. 33, no. 3, pp. 2696–2705, may 2018.

[11] M. E. Samper and A. Vargas, "Investment decisions in distribution networks under uncertainty with distributed generation—part ii: Implementation and results," *IEEE Transactions on Power Systems*, vol. 28, no. 3, pp. 2341–2351, aug 2013.

[12] M. Lavorato, M. J. Rider, A. V. Garcia, and R. Romero, "A constructive heuristic algorithm for distribution system planning," *IEEE Transactions on Power Systems*, vol. 25, no. 3, pp. 1734–1742, aug 2010.

[13] The European Parliament and the Council of the European Union, "Directive (EU) 2019/944 of the European Parliament and of the Council of 5 June 2019 on common rules for the internal market for electricity and amending Directive 2012/27/EU," *Official Journal of the European Union*, 2019, l 158/125.

[14] ACER, *Report on Distribution Tariff Methodologies in Europe*, European Union Agency for the Cooperation of Energy Regulators, Ljubljana, Slovenia, feb 2021.

[15] M. Cornet, G. Bailly, M. Glavic, and B. Cornélusse, "A one-leader multi-follower approach to distribution network development planning," in *2023 IEEE PES Innovative Smart Grid Technologies Europe (ISGT EUROPE)*, Grenoble, France, 2023, pp. 1–5.

[16] S. Mathieu, Q. Louveaux, D. Ernst, and B. Cornélusse, "Dsima: A testbed for the quantitative analysis of interaction models within distribution networks," *Sustainable Energy, Grids and Networks*, vol. 5, pp. 78–93, 2016.

[17] M. E. Baran and F. F. Wu, "Network reconfiguration in distribution systems for loss reduction," *IEEE Transactions on Power Delivery*, vol. 4, no. 2, pp. 1401–1407, Apr 1989.

[18] K. Poncelet, H. Höschle, E. Delarue, A. Virag, and W. D'haeseleer, "Selecting representative days for capturing the implications of integrating intermittent renewables in generation expansion planning problems," *IEEE Transactions on Power Systems*, vol. 32, no. 3, pp. 1936–1948, 2017.

[19] M. A. Mejia, L. H. Macedo, G. Muñoz-Delgado, J. Contreras, and A. Padilha-Feltrin, "Multistage planning model for active distribution systems and electric vehicle charging stations considering voltage-dependent load behavior," *IEEE Transactions on Smart Grid*, vol. 13, no. 2, pp. 1383–1397, 2022.

APPENDIX

Sets

$p \in \mathcal{P}$	Discrete time steps
$b \in \mathcal{B}$	Load buses
$s_{hv} \in \mathcal{S}_{HV}$	HV substations
$s_{mv} \in \mathcal{S}_{MV}$	MV substations
$c \in \mathcal{C}$	Conductor types
$l_{ij} \in \mathcal{L}$	Candidate power lines
$l_k \in \mathcal{L}_k^{\text{to/from}}$	Lines to/from bus k
$l_{s_{mv}} \in \mathcal{L}_{s_{mv}}^{\text{to/from LV}}$	LV lines to/from s_{mv}
$j \in \mathcal{J}$	All nodes ($\mathcal{B} \cup \mathcal{S}_{HV} \cup \mathcal{S}_{MV}$)

Parameters

$P_{load,p,b}$	Active power demand at bus b, period p [MW]
$Q_{load,p,b}$	Reactive power demand at bus b, period p [Mvar]
I_p	Solar irradiance at period p [MW/m^2]
$r_{l,c}$	Resistance of line l with conductor c [kΩ]
$x_{l,c}$	Reactance of line l with conductor c [kΩ]
$I_{max,c}$	Max current rating of conductor c [kA]
V_{min}	Minimum voltage [V]
V_{max}	Maximum voltage [V]
A_b^{max}	Max PV installation at bus b [m^2]
$\pi_{s_{hv}}$	HV substation capacity cost [k€/MVA]
$\pi_{s_{mv}}$	MV substation capacity cost [k€/MVA]
π_{scom}	Statcom capacity cost [k€/Mvar]
π_{pv}	PV capacity cost [k€/m^2]
$\pi_{storage}$	Storage capacity cost [k€/kWh]
$\pi_{inverter}$	Inverter capacity cost [k€/kVA]
$f_{s_{hv}}$	HV substation installation cost [k€]
$f_{s_{mv}}$	MV substation installation cost [k€]
f_{scom}	Statcom installation cost [k€]
f_{pv}	PV installation cost [k€]
$f_{storage}$	Storage installation cost [k€]
$f_{inverter}$	Inverter installation cost [k€]
π_{import}	Energy import cost [k€/MWh]
π_{export}	Energy export cost [k€/MWh]
π_{losses}	Energy losses cost [k€/MWh]
$\eta_{storage}$	Storage efficiency

Variables

α_l	Line l activation
$\delta_{l,c}$	Conductor c choice in line l
$\beta_{s_{hv}}$	HV substation s_{hv} activation
$\gamma_{s_{mv}}$	MV substation s_{mv} activation
μ_b	Statcom at bus b activation
$S_{s_{hv}}$	HV substation s_{hv} capacity [MVA]
$S_{s_{mv}}$	MV substation s_{mv} capacity [MVA]
Q_{scom_b}	Statcom at bus b capacity [Mvar]
π_b	PV installation at bus b option
σ_b	Storage installation at bus b option
$A_{pv,b}$	PV capacity at bus b [m^2]
$S_{inv,b}$	Inverter capacity at bus b [kVA]
$E_{stor,b}$	Storage capacity at bus b [kWh]
$P_{p,l}$	Active power flow in line l at period p [MW]
$Q_{p,l}$	Reactive power flow in line l at period p [MW]
$i^2_{p,l}$	Current squared in line l at period p [kA]
$P_{p,l,c}$	Active power flow by conductor c [MW]
$Q_{p,l,c}$	Reactive power flow by conductor c [Mvar]
$i^2_{p,l,c}$	Current squared by conductor c [kA]
$v^2_{p,j}$	Voltage squared at node j [V]
$P_{p,s_{mv}}$	Active power flow through MV substation s_{mv} at period p [MW]
$Q_{p,s_{mv}}$	Reactive power flow at MV substation s_{mv} at period p [Mvar]
$P_{p,s_{hv}}$	Active power flow through HV substation s_{hv} at period p [MW]
$Q_{p,s_{hv}}$	Reactive power flow at HV substation s_{hv} at period p [Mvar]
$Q_{scom,p,b}$	Reactive power produced by statcom at bus b at period p [Mvar]
$\Delta i^2_{p,l,c}$	Overcurrent slack for line l, conductor c, period p [kA]
$P_{bus,p,b}$	Net active power injection at bus b, period p [MW]
$Q_{bus,p,b}$	Net reactive power injection at bus b, period p [Mvar]
$P_{pv,p,b}$	PV production at bus b, period p [kW]
$E_{p,b}$	Storage energy at bus b, period p [kWh]
$P_{ch,p,b}$	Storage charging power at bus b, period p [kW]
$P_{dis,p,b}$	Storage discharging power at bus b, period p [kW]
$P_{inv,p,b}$	Inverter active power at bus b, period p [kW]
$Q_{inv,p,b}$	Inverter reactive power at bus b, period p [kVar]
$\hat{\gamma}_{s_{mv}}$	MV substation s_{mv} topology activation
F_l	Fictitious power flow in line l
$F_{unserved,b}$	Unserved fictitious power at bus b
$F_{s_{hv}}$	Fictitious power capacity of HV substation s_{hv}